AIAA JOURNAL
Vol. 39, No. 11, November 2001

Active and Passive Suppressions of Nonlinear Panel Flutter Using Finite Element Method

Seong Hwan Moon* and Seung Jo Kim†
Seoul National University, Seoul 151-742, Republic of Korea

Active and passive suppression schemes for nonlinear flutter of composite panel are investigated using lead zirconate titanate (PZT). First, in the active control method, the optimal controller based on the linear optimal control theory is designed for flutter suppression of the panel. Second, a new approach, a passive suppression scheme, is suggested for suppression of the nonlinear panel flutter. A passive damping technology, using one shunt circuit and two independent shunt circuits, which is believed to be a more robust suppression system in practical operation, is proposed. This approach requires very little or no electrical power. In this passive method, the piezoelectric shunt circuit, which consists of resistor–inductor–capacitor elements in series, is applied. In both methods, a finite element formulation for composite plates with PZT layers is derived using classical laminated plate theory. The adopted aerodynamic theory is based on the quasi-steady piston theory, and the von Kármán nonlinear strain-displacement relation is used. A modal reduction technique is used to reduce the number of modes involved and to simplify the nonlinearity of the model. Numerical results, which are based on the reduced nonlinear modal equations of active and passive suppression for nonlinear panel flutter are presented in the time domain using the Newmark-ß method. To achieve the best suppression effect, optimal shape and location of the piezoceramic (PZT) patches are determined by using genetic algorithms. The results clearly demonstrate that the passive damping scheme as well as active control can effectively attenuate the flutter.

Nomenclature

a	=	panel length
b	=	panel width
$\boldsymbol{c}$	=	elastic stiffness matrix
D	=	electrical displacement (charge/area in the z direction)
$\boldsymbol{d}$, d_{31}	=	piezoelectric constants (strain/charge)
E_3	=	voltage per unit length
$\boldsymbol{e}$	=	piezoelectric constant matrix
g_a	=	nondimensional aerodynamic damping
h	=	panel thickness
$\boldsymbol{h}$	=	piezoelectric constant matrix
L	=	inductance
p_a	=	freestream aerodynamic pressure
Q	=	charge
$\bar{Q}_{ij}$	=	transformed reduced stiffness matrix
R	=	resistance
u, v, w	=	displacements
V_3	=	voltage applied to the actuator
V_∞	=	freestream velocity
α	=	thermal expansion coefficient
$\Delta T(x, y, z)$	=	temperature change
ε, $\{\varepsilon\}$	=	strain vectors
$\boldsymbol{\kappa}$, $\{k\}$	=	curvature vector
λ	=	nondimensional aerodynamic pressure
ρ	=	mass density
$\boldsymbol{\sigma}$, $\{\sigma\}$	=	stress vectors
τ	=	nondimensional time, $\omega_0 t$
Φ	=	normal mode vector

Subscripts

a	=	air
b	=	bending
h	=	host structure (composite plate)
m	=	membrane
p	=	piezoelectric material
θ	=	nonlinear

Superscripts

D	=	constant electric displacement
E	=	constant electric field
S	=	constant strain
T	=	transpose
t	=	constant stress

Received 19 May 2000; revision received 20 April 2001; accepted for publication 29 April 2001.

*Research Assistant, Department of Aerospace Engineering, San 56-1, Shinrim-Dong, Kwanak-Gu. Student Member AIAA.

†Professor, Department of Aerospace Engineering, San 56-1, Shinrim-Dong, Kwanak-Gu. Member AIAA.

I. Introduction

PANEL flutter is a self-excited aeroelastic phenomenon. It is caused and maintained by the interactions between motions of an aircraft structural panel and aerodynamic loads exerted on that panel. It occurs most frequently in high-speed, most often transonic, supersonic and hypersonic flow. The presence of high temperature by aerodynamic heating causes the panel stiffness to reduce, which enables flutter motions to occur at lower dynamic pressures than in the case without thermal influence.

Linear analysis on panel flutter provides information about airflow speed at which the panel becomes dynamically unstable and the amplitude of oscillation grows exponentially with time. In reality, the nonlinear effect of the panel appears as the amplitude grows to a certain level, and the vibration reaches a limited value (so-called limit cycle).

Much research on the suppression of nonlinear panel flutter has been carried out by using the piezoelectric material or shape memory alloy. Scott and Weisshaar[1] performed active suppression research on increasing the flutter velocity using the piezoceramic and shape memory alloys with a linear plate theory and the Ritz method. Zhou et al.[2] used a finite element method to suppress nonlinear panel flutter under uniform thermal loading by using a modal reduction scheme and linear quadratic regulator linear control. The feasibility of passively dissipating mechanical energy with electrical shunt circuits has been investigated. Hagood and Von Flotow[3] formulated the equations of the mechanical and electrical characteristics with piezoelectric material shunted with electrical circuits for the case of a resistor alone and a inductor–resistor resonant shunt to provide damping for the beam. Hollkamp[4] showed that multiple modes could be suppressed using a single piezoelectric patch connected to the

multiple inductor–resistor–capacitor for a beam model. Tang et al.[5] showed that a structural vibration could be suppressed effectively using the active–passive hybrid piezoelectric network for the beam model. However, most of the previous papers on resonant-shunted piezoelectrics have the limitation in that the theories are applied to a uniaxial loading condition such as beams. For more complex structures and loading conditions, the theory should be modified to give reasonable solutions. Hollkamp and Gordon[6] investigated a suppression scheme for a two-dimensional planar problem using a passive piezoelectric network. Lag mode suppression of hingeless helicopter rotor blade was investigated by passive piezoelectric damping.[7]

In this paper, the governing equations of the electromechanically coupled panel subjected to a thermal load are derived for active and passive suppression. They are based on the extended Hamilton's principle, on the classical laminated plate theory, and the von Kármán plate model for the panel structure and quasi-steady first-order piston theory for the supersonic airflow. A finite element discretization is carried out by using the four-node conforming plate element. There are two in-plane degrees of freedom and four bending degrees of freedom at each node. The Lagrange polynomial and Hermite polynomial are used to interpolate each of the in-plane and bending displacements, respectively. A modal reduction technique is used to reduce the number of modes involved and to simplify the nonlinearity of the model with first six modes in the airflow direction and only the first mode in the spanwise direction. Numerical results, which are based on the reduced nonlinear modal equations, of active and passive suppression for nonlinear panel flutter are presented in the time domain by using the Newmark-ß method (see Ref. 8). To achieve the best suppression effect, optimal shape and location of the piezoceramic [lead zirconate titanate (PZT)] patches are determined by using genetic algorithms.[9]

First, in the active control method, the optimal controller based on the linear optimal control theory is designed for flutter suppression of the panel. Second, a passive approach is suggested for suppression of the nonlinear panel flutter. A passive damping technology, which is believed to be a more robust suppression system in practical operation, and in which there are no need for power equipment, sensor systems, and controller, is simulated by using one shunt circuit and two independent shunt circuits. Optimal resistance and inductance are determined by a pole placement method to suppress the vibration effectively.

II. Constitutive Equations

The linear piezoelectric constitutive equations of a piezoelectric material can be written as follows.

Active control:

$$\boldsymbol{\sigma} = \boldsymbol{c}^E\boldsymbol{\varepsilon} - \boldsymbol{e}^T\boldsymbol{E}, \qquad \boldsymbol{D} = \boldsymbol{e}\boldsymbol{\varepsilon} + \in^S \boldsymbol{E} \tag{1}$$

Passive damping:

$$\boldsymbol{\sigma} = \boldsymbol{c}^D\boldsymbol{\varepsilon} - \boldsymbol{h}^T\boldsymbol{D}, \qquad \boldsymbol{E} = -\boldsymbol{h}\boldsymbol{\varepsilon} + \boldsymbol{\beta}^S\boldsymbol{D} \tag{2}$$

where $\boldsymbol{E}$ is the electric field vector (volts/length along the transverse direction), $\boldsymbol{D}$ is the electric displacement vector (charge/area in the transverse direction), and $\in^S$ represents the dielectric constant matrix at a constant strain.

A piezo stress/charge constant $\boldsymbol{e}$ is $\boldsymbol{e} = \boldsymbol{c}^E\boldsymbol{d}$. The PZT material is approximately isotropic in the in-plane directions.[6] For piezoceramic material (PZT) polarized in the thickness direction (3 direction), impermittivity components $\boldsymbol{\beta}^S$ are expressed as follows:

$$\beta^s = \begin{bmatrix} 1/\in_{11}^S & 0 & 0 \\ 0 & 1/\in_{11}^S & 0 \\ 0 & 0 & 1/\in_{33}^S \end{bmatrix} \tag{3}$$

and piezoelectric constant matrix $\boldsymbol{h}$ can be expressed as follows:

$$\boldsymbol{h} = \begin{bmatrix} 0 & 0 & 0 & 0 & h_{15} & 0 \\ 0 & 0 & 0 & h_{15} & 0 & 0 \\ h_{31} & h_{31} & h_{31} & 0 & 0 & 0 \end{bmatrix} \tag{4}$$

For piezoelectric material under plane stress, the piezoelectric constant matrices $\boldsymbol{g}$ and $\boldsymbol{h}$ can be expressed as follows:

$$\boldsymbol{g} = \boldsymbol{\beta}^t\boldsymbol{d} = \beta_{33}^t[d_{31} \quad d_{31} \quad 0] = d_{31}/\in_{33}^t [1 \quad 1 \quad 0] \tag{5}$$

$$\boldsymbol{h} = \boldsymbol{g}\boldsymbol{c}^D = \left[d_{31}\left(C_{11}^D + C_{12}^D\right)\Big/ \in_{33}^t\right][1 \quad 1 \quad 0] = [h_{31} \quad h_{31} \quad 0] \tag{6}$$

The PZT material is approximately isotropic in the in-plane directions ($d_{31} = d_{32}$) (Ref. 3). Then, the stress–strain relationships of the piezoceramic layer subjected to a temperature variation $\Delta T(x, y, z)$ due to aerodynamic heating in supersonic flow is expressed as follows.

Active control:

$$\begin{Bmatrix} \sigma_x \\ \sigma_y \\ \tau_{xy} \end{Bmatrix} = \begin{bmatrix} \bar{Q}_{11} & \bar{Q}_{12} & \bar{Q}_{16} \\ \bar{Q}_{12} & \bar{Q}_{22} & \bar{Q}_{26} \\ \bar{Q}_{16} & \bar{Q}_{26} & \bar{Q}_{66} \end{bmatrix}_p \left[\begin{Bmatrix} \varepsilon_x \\ \varepsilon_y \\ \gamma_{xy} \end{Bmatrix} - \Delta T \begin{Bmatrix} \alpha \\ \alpha \\ 0 \end{Bmatrix}_p - E_3 \begin{Bmatrix} d_{31} \\ d_{31} \\ 0 \end{Bmatrix}^E \right] \tag{7}$$

Passive damping:

$$\begin{Bmatrix} \sigma_x \\ \sigma_y \\ \tau_{xy} \end{Bmatrix} = \begin{bmatrix} \bar{Q}_{11} & \bar{Q}_{12} & \bar{Q}_{16} \\ \bar{Q}_{12} & \bar{Q}_{22} & \bar{Q}_{26} \\ \bar{Q}_{16} & \bar{Q}_{26} & \bar{Q}_{66} \end{bmatrix}_p \left[\begin{Bmatrix} \varepsilon_x \\ \varepsilon_y \\ \gamma_{xy} \end{Bmatrix} - \Delta T \begin{Bmatrix} \alpha \\ \alpha \\ 0 \end{Bmatrix}_p \right] - D_3 \begin{Bmatrix} h_{31} \\ h_{31} \\ 0 \end{Bmatrix}^D, \qquad E_3 = \frac{1}{\in_{33}^S} D_3 - [h_{31} \quad h_{31} \quad 0] \begin{Bmatrix} \varepsilon_x \\ \varepsilon_y \\ \gamma_{xy} \end{Bmatrix} \tag{8}$$

For a piezoceramic material, $\bar{Q}_{ij}$ (transformed reduced stiffness matrix) is given as

$$[\bar{Q}_{ij}]_p = \left(\frac{E}{1-v^2}\right)_P \begin{bmatrix} 1 & v & 0 \\ v & 1 & 0 \\ 0 & 0 & \dfrac{1-v}{2} \end{bmatrix}_p \tag{9}$$

For a kth layer of a composite plate, the constitutive equations based on the plane stress state can be written as follows:

$$\begin{Bmatrix} \sigma_x \\ \sigma_y \\ \tau_{xy} \end{Bmatrix}_h^k = \begin{bmatrix} \bar{Q}_{11} & \bar{Q}_{12} & \bar{Q}_{16} \\ \bar{Q}_{12} & \bar{Q}_{22} & \bar{Q}_{26} \\ \bar{Q}_{16} & \bar{Q}_{26} & \bar{Q}_{66} \end{bmatrix}_h^k \left\{ \begin{Bmatrix} \varepsilon_x \\ \varepsilon_y \\ \gamma_{xy} \end{Bmatrix} - \Delta T \begin{Bmatrix} \alpha_x \\ \alpha_y \\ \alpha_{xy} \end{Bmatrix}_h^k \right\} \tag{10}$$

The dynamic equilibrium equation of the composite plate integrated with the piezoelectric patches is derived based on the classical laminated plate theory (CLPT), which is an extension of Kirchhoff plate theory to laminated composite plate. According to CLPT, the displacement field u, v, and w is expressed as

$$u(x, y, z, t) = u_0(x, y, t) - z\frac{\partial w}{\partial x}$$

$$v(x, y, z, t) = v_0(x, y, t) - z\frac{\partial w}{\partial y}$$

$$w(x, y, z, t) = w_0(x, y, t) \tag{11}$$

where u_0, v_0, and w_0 are the displacement fields of a point on the midplane of the laminate. A laminate coordinate system is assumed such that x and y are the in-plane axes, and the z direction coincides with the thickness direction of the laminate.

Von Kármán's nonlinear strain-displacement relationships are written as follows:

$$\varepsilon = \begin{Bmatrix} \varepsilon_x \\ \varepsilon_y \\ \gamma_{xy} \end{Bmatrix} = \begin{Bmatrix} u_{0,x} \\ v_{0,y} \\ u_{0,x} + v_{0,y} \end{Bmatrix} + \frac{1}{2}\begin{Bmatrix} w_{,x}^2 \\ w_{,y}^2 \\ 2w_{,x}w_{,y} \end{Bmatrix} - z\begin{Bmatrix} w_{,xx} \\ w_{,yy} \\ 2w_{,xy} \end{Bmatrix} = \varepsilon_m + \varepsilon_\theta + z\boldsymbol{k} \tag{12}$$

where u and v are the membrane displacements, ε_m is linear membrane strain vector, and ε_θ is the nonlinear membrane strain vector due to large deflections.

III. Aerodynamic Theory

The transverse forces acting on the panel under sufficiently high supersonic Mach number ($M > 1.7$) and zero flow angle can be suitably described by quasi-steady first-order piston theory[2] as

$$p_a = -\frac{\rho_a V_\infty^2}{\beta}\left\{\frac{\partial w}{\partial x} + \left(\frac{M_\infty^2 - 2}{M_\infty^2 - 1}\right)\frac{1}{V_\infty}\frac{\partial w}{\partial t}\right\} = -\left(\lambda\frac{D_{110}}{a^3}\frac{\partial w}{\partial x} + \frac{g_a}{\omega_0}\frac{D_{110}}{a^4}\frac{\partial w}{\partial t}\right) \tag{13}$$

where the parameter β is defined as $\beta = (M_\infty^2 - 1)^{1/2}$. D_{110} is the first entry of the laminate bending stiffness matrix calculated when all of the fibers of the composite layers are aligned in the direction of the airflow.

The nondimensional aerodynamic pressure parameter λ and nondimensional aerodynamic damping g_a can be expressed as follows:

$$\lambda = \frac{\rho_a V_\infty^2 a^3}{\beta D_{110}}, \qquad g_a = \frac{\rho_a V_\infty \left(M_\infty^2 - 2\right)}{\rho h \omega_0 \beta^3} \tag{14}$$

where ρ is the mass density of the panel.

A convenient reference frequency is defined by

$$\omega_0 = \sqrt{D_{110}/\rho h a^4} \tag{15}$$

Nondimensional mass parameters such as air-panel mass ratio and aerodynamic damping coefficient are introduced as

$$\mu = \frac{\rho_a a}{\rho h}, \qquad c_a = \left(\frac{M_\infty^2 - 2}{M_\infty^2 - 1}\right)^2\frac{\mu}{\beta} \tag{16}$$

For Mach number $M_\infty \gg 1$,

$$g_a = \sqrt{(\lambda c_a)}, \qquad c_a = \mu/M_\infty \tag{17}$$

IV. Governing Equations

For an electromechanically coupled system, the equations of motion can be derived using Hamilton's principle:

$$\delta\Pi = \int_{t_1}^{t_2}[\delta(T - U) + \delta W]\,\mathrm{d}t = 0 \tag{18}$$

where

$$T = \frac{1}{2}\int_{V_h}\rho_h\left(\dot{u}_0^2 + \dot{v}_0^2 + \dot{w}^2\right)\mathrm{d}V + \frac{1}{2}\int_{V_p}\rho_p\left(\dot{u}_0^2 + \dot{v}_0^2 + \dot{w}^2\right)\mathrm{d}V \tag{19}$$

Active control:

$$U = \frac{1}{2}\int_{V_h}\varepsilon^T\boldsymbol{\sigma}_h\,\mathrm{d}V + \frac{1}{2}\int_{V_p}\varepsilon^T\boldsymbol{\sigma}_p\,\mathrm{d}V \tag{20}$$

Passive damping:

$$U = \frac{1}{2}\int_{V_h}\varepsilon^T\boldsymbol{\sigma}_h\,\mathrm{d}V + \frac{1}{2}\int_{V_p}\varepsilon^T\boldsymbol{\sigma}_p\,\mathrm{d}V + \frac{1}{2}\int_{V_p}D_3E_3\,\mathrm{d}V \tag{21}$$

where T is the kinetic energy of the integrated system and U is the potential energy that consists of strain energy and electrical energy.

The virtual work due to the aerodynamic pressure and electric potential is described as follows.

Active control:

$$\delta W = \int_A \delta w^T p_a\,\mathrm{d}A \tag{22}$$

Passive damping:

$$\delta W = (-L\ddot{Q} - R\dot{Q})\,\delta Q + \int_A \delta w^T p_a\,\mathrm{d}A \tag{23}$$

Then, the potential energy is given as follows.

Active control:

$$\delta U = \int_V\Big[\delta\varepsilon_m^T\bar{\boldsymbol{Q}}\varepsilon_m + \delta\varepsilon_m^T\bar{\boldsymbol{Q}}\varepsilon_\theta + \delta\varepsilon_m^T\bar{\boldsymbol{Q}}z\boldsymbol{k} + \delta\varepsilon_\theta^T\bar{\boldsymbol{Q}}\varepsilon_m + \delta\varepsilon_\theta^T\bar{\boldsymbol{Q}}\varepsilon_\theta + \delta\varepsilon_\theta^T\bar{\boldsymbol{Q}}z\boldsymbol{k} + z\delta\boldsymbol{k}^T\bar{\boldsymbol{Q}}\varepsilon_m + z\delta\boldsymbol{k}^T\bar{\boldsymbol{Q}}\varepsilon_\theta + z\delta\boldsymbol{k}^T\bar{\boldsymbol{Q}}z\boldsymbol{k} + \delta\varepsilon_m^T\bar{\boldsymbol{Q}}\Delta T\boldsymbol{\alpha} - \delta\varepsilon_\theta^T\bar{\boldsymbol{Q}}\Delta T\boldsymbol{\alpha} - z\delta k^T\Delta T\bar{\boldsymbol{Q}}\boldsymbol{\alpha} - \delta\varepsilon_m^T E_3\bar{\boldsymbol{Q}}\boldsymbol{d} - \delta\varepsilon_\theta^T E_3\bar{\boldsymbol{Q}}\boldsymbol{d} - z\delta\boldsymbol{k}^T E_3\bar{\boldsymbol{Q}}\boldsymbol{d}\Big]\,\mathrm{d}V \tag{24}$$

Passive damping:

$$\delta U = \int_V\Big[\delta\varepsilon_m^T\bar{\boldsymbol{Q}}\varepsilon_m + \delta\varepsilon_m^T\bar{\boldsymbol{Q}}\varepsilon_\theta + \delta\varepsilon_m^T\bar{\boldsymbol{Q}}z\boldsymbol{k} + \delta\varepsilon_\theta^T\bar{\boldsymbol{Q}}\varepsilon_m + \delta\varepsilon_\theta^T\bar{\boldsymbol{Q}}\varepsilon_\theta + \delta\varepsilon_\theta^T\bar{\boldsymbol{Q}}_m z\boldsymbol{k} + z\delta\boldsymbol{k}^T\bar{\boldsymbol{Q}}\varepsilon_m + z\delta\boldsymbol{k}^T\bar{\boldsymbol{Q}}\varepsilon_\theta + z\delta\boldsymbol{k}^T\bar{\boldsymbol{Q}}z\boldsymbol{k} + \delta\varepsilon_m^T\bar{\boldsymbol{Q}}\Delta T\boldsymbol{\alpha} - \delta\varepsilon_\theta^T\,\Delta T\bar{\boldsymbol{Q}}\boldsymbol{\alpha} - z\delta\boldsymbol{k}^T\Delta T\bar{\boldsymbol{Q}}\boldsymbol{\alpha} - \delta\varepsilon_m^T\boldsymbol{h}^T D_3 - \delta\varepsilon_\theta^T\boldsymbol{h}^T D_3 - z\delta\boldsymbol{k}^T\boldsymbol{h}^T D_3 + \underline{\delta D_3^T\frac{1}{\in_{33}^S}D_3} - \underline{\delta D_3^T h_{31}\varepsilon_x} - \underline{\delta D_3^T h_{31}\varepsilon_y}\Big]\,\mathrm{d}V \tag{25}$$

where $\boldsymbol{d} = d_{31}[1\ \ 1\ \ 0]^T$ for PZT layers, $\boldsymbol{\alpha} = [\alpha_x\ \ \alpha_y\ \ \alpha_{xy}]_h^T$ for composite plate layers, and $\boldsymbol{\alpha} = \alpha_p[1\ \ 1\ \ 0]^T$ for PZT layers. In Eq. (25), underlined terms are derived from electrical energy.

A four-node conforming plate element is employed in this study. There are two in-plane degrees of freedom, u and v, and four bending degrees of freedom, w, $w_{,x}$, $w_{,y}$, and $w_{,xy}$, at each node:

$$\boldsymbol{w}_b^e = \{w_1, w_{1x}, w_{1y}, w_{1xy}, w_2, w_{2x}, w_{2y}, w_{2xy}, w_3, w_{3x}, w_{3y}w_{3xy}, w_4, w_{4x}, w_{4y}, w_{4xy}\}^T, \quad \boldsymbol{w}_m^e = \{u_1, v_1, u_2, v_2, u_3, v_3, u_4, v_4\}^T \tag{26}$$

The Lagrange polynomial and Hermite polynomial are used to interpolate each of the in-plane and bending displacements, respectively. The displacements u_0, v_0, and w can be expressed by nodal degrees of freedom as follows:

$$\begin{Bmatrix} u_0 \\ v_0 \end{Bmatrix} = \begin{Bmatrix} \boldsymbol{N}_{mx} \\ \boldsymbol{N}_{my} \end{Bmatrix}\boldsymbol{w}_m^e = \boldsymbol{N}_m\boldsymbol{w}_m^e, \qquad w = \boldsymbol{N}_b\boldsymbol{w}_b^e \tag{27}$$

The membrane strain components and curvatures can be expressed in terms of the nodal degrees of freedom:

$$\varepsilon_m\begin{Bmatrix} \boldsymbol{B}_{mx} \\ \boldsymbol{B}_{my} \\ \boldsymbol{B}_{mxy} \end{Bmatrix}\boldsymbol{w}_m^e = \boldsymbol{B}_m\boldsymbol{w}_m^e$$

$$\varepsilon_\theta = \frac{1}{2}\begin{Bmatrix} \left(\frac{\partial w}{\partial x}\right)^2 \\ \left(\frac{\partial w}{\partial y}\right)^2 \\ 2\frac{\partial w}{\partial x}\frac{\partial w}{\partial y} \end{Bmatrix} = \frac{1}{2}\begin{Bmatrix} \left(\frac{\partial \boldsymbol{N}_b}{\partial x}\boldsymbol{w}_b^e\right)^2 \\ \left(\frac{\partial \boldsymbol{N}_b}{\partial y}\boldsymbol{w}_b^e\right)^2 \\ 2\frac{\partial \boldsymbol{N}_b}{\partial x}\boldsymbol{w}_b^e\frac{\partial \boldsymbol{N}_b}{\partial y}\boldsymbol{w}_b^e \end{Bmatrix}$$

$$= \frac{1}{2}\begin{Bmatrix} \left(\boldsymbol{B}_{\theta x}\boldsymbol{w}_b^e\right)^2 \\ \left(\boldsymbol{B}_{\theta y}\boldsymbol{w}_b^e\right)^2 \\ 2\boldsymbol{B}_{\theta x}\boldsymbol{w}_b^e\boldsymbol{B}_{\theta y}\boldsymbol{w}_b^e \end{Bmatrix} = \frac{1}{2}\begin{Bmatrix} \boldsymbol{w}_b^{eT}\boldsymbol{B}_{\theta x}^T\boldsymbol{B}_{\theta x}\boldsymbol{w}_b^e \\ \boldsymbol{w}_b^{eT}\boldsymbol{B}_{\theta y}^T\boldsymbol{B}_{\theta y}\boldsymbol{w}_b^e \\ 2\boldsymbol{w}_b^{eT}\boldsymbol{B}_{\theta x}^T\boldsymbol{B}_{\theta y}\boldsymbol{w}_b^e \end{Bmatrix}$$

$$\boldsymbol{k} = \begin{Bmatrix} -\dfrac{\partial^2 \boldsymbol{N}_b}{\partial x^2}\boldsymbol{w}_b^e \\ -\dfrac{\partial^2 \boldsymbol{N}_b}{\partial y^2}\boldsymbol{w}_b^e \\ -2\dfrac{\partial^2 \boldsymbol{N}_b}{\partial x\,\partial y}\boldsymbol{w}_b^e \end{Bmatrix} = \begin{Bmatrix} \boldsymbol{B}_{kx} \\ \boldsymbol{B}_{ky} \\ \boldsymbol{B}_{kxy} \end{Bmatrix} \boldsymbol{w}_b^e = \boldsymbol{B}_k \boldsymbol{w}_b^e \tag{28}$$

and the virtual membrane strains and curvatures are expressed as follows:

$$\delta\boldsymbol{\varepsilon}_m = \boldsymbol{B}_m \delta \boldsymbol{w}_m^e$$

$$\delta\boldsymbol{\varepsilon}_\theta = \begin{Bmatrix} \boldsymbol{w}_b^{eT}\boldsymbol{B}_{\theta x}^T\boldsymbol{B}_{\theta x}\delta\boldsymbol{w}_b^e \\ \boldsymbol{w}_b^{eT}\boldsymbol{B}_{\theta y}^T\boldsymbol{B}_{\theta y}\delta\boldsymbol{w}_{bb}^e \\ \boldsymbol{w}_b^{eT}\boldsymbol{B}_{\theta x}^T\boldsymbol{B}_{\theta y}\delta\boldsymbol{w}_b^e + \boldsymbol{w}_b^{eT}\boldsymbol{B}_{\theta y}^T\boldsymbol{B}_{\theta x}\delta\boldsymbol{w}_b^e \end{Bmatrix}$$

$$\delta\boldsymbol{k} = \boldsymbol{B}_k \delta \boldsymbol{w}_b^e \tag{29}$$

The electrical displacement D_3 is the generated charge per area A_p of a piezoelectric material. It is assumed that electric displacement D_3 is constant along the thickness direction:

$$D_3 = Q/A_p \tag{30}$$

When Eqs. (26–30) are used, the element matrices can be obtained. The detailed expressions of these element matrices for active control method are found in Ref. 2. For passive suppression method, the element matrices that relate to electric charge can be written as follows:

$$-\int_V \delta\boldsymbol{\varepsilon}_m^T \boldsymbol{h}^T D_3 \,\mathrm{d}V = \delta\boldsymbol{w}_m^{eT}\boldsymbol{H}_{mq}^{(e)} Q \tag{31}$$

$$-\int_V \delta\boldsymbol{\varepsilon}_\theta^T \boldsymbol{h}^T D_3 \,\mathrm{d}V = \delta\boldsymbol{w}_b^{eT}\boldsymbol{H}1_{bq}^{(e)} Q + \delta\boldsymbol{w}_b^{eT}\boldsymbol{K}1_{bbq}^{(e)}\boldsymbol{w}_b^e \tag{32}$$

$$-\int_V z\delta\boldsymbol{k}^T \boldsymbol{h}^T D_3 \,\mathrm{d}V = \delta\boldsymbol{w}_b^{eT}\boldsymbol{H}1_{bq}^{(e)} Q \tag{33}$$

$$\int_V \delta D_3^T \frac{1}{\epsilon_{33}^S} D_3 \,\mathrm{d}V = \delta Q \frac{1}{C_p^S} Q \tag{34}$$

$$\int_V -\delta D_3^T h_{31}\varepsilon_x - \delta D_3^T h_{31}\varepsilon_y \,\mathrm{d}V = \delta Q^T \boldsymbol{H}_{qm}^{(e)}\boldsymbol{w}_m^e + \delta Q^T \boldsymbol{H}_{qb}^{(e)}\boldsymbol{w}_b^e + \delta Q^T \boldsymbol{H}1_{qb}^{(e)}\boldsymbol{w}_b^e \tag{35}$$

where $\boldsymbol{H}$ is the coupling matrix between electrical and mechanical motion and is expressed as follows:

$$\boldsymbol{H}_{bq}^e = -\int_{V_p} \frac{z\boldsymbol{B}_k^T\boldsymbol{h}^T}{A_p}\,\mathrm{d}V, \qquad \boldsymbol{H}_{mq}^e = -\int_{V_p} \frac{\boldsymbol{B}_m^T\boldsymbol{h}^T}{A_p}\,\mathrm{d}V$$

$$\boldsymbol{H}1_{bq}^e = -\frac{1}{2}\int_{V_p} \frac{h_{31}\left(\boldsymbol{B}_{\theta x}^T\boldsymbol{B}_{\theta x}\boldsymbol{w}_b^e + \boldsymbol{B}_{\theta y}^T\boldsymbol{B}_{\theta y}\boldsymbol{w}_b^e\right)}{A_p}\,\mathrm{d}V \tag{36}$$

and $\boldsymbol{K}1_{bbq}^e(\mathrm{Q})$ is the stiffness matrix that linearly depends on the electrical charge and is written as follows:

$$\boldsymbol{K}1_{bbq}^e(Q) = -\frac{1}{2}\int_{V_p} \frac{h_{31}\left(\boldsymbol{B}_{\theta x}^T\boldsymbol{B}_{\theta x}Q + \boldsymbol{B}_{\theta y}^T\boldsymbol{B}_{\theta y}Q\right)}{A_p}\,\mathrm{d}V \tag{37}$$

After assembling the element matrices, we obtain the following discretized governing equations for the passive suppression method:

$$\boldsymbol{M}_b\ddot{\boldsymbol{W}}_b + \boldsymbol{G}\dot{\boldsymbol{W}}_b + \left[\lambda\boldsymbol{A} + \boldsymbol{K}_b + \boldsymbol{K}_{N\Delta T} + \boldsymbol{K}1_{bbq}(Q) + \boldsymbol{K}1_{bbb}(\boldsymbol{W}_b) + \boldsymbol{K}1_{bbm}(\boldsymbol{W}_b) + \boldsymbol{K}2_b\left(\boldsymbol{W}_b^2\right)\right]\boldsymbol{W}_b + [\boldsymbol{K}_{bm} + \boldsymbol{K}1_{bm}(\boldsymbol{W}_b)]\boldsymbol{W}_m = \boldsymbol{P}_{b\Delta T} - \boldsymbol{H}_{bq}\boldsymbol{Q} - \boldsymbol{H}1_{bq}(\boldsymbol{W}_b) \tag{38}$$

$$\boldsymbol{M}_m\ddot{\boldsymbol{W}}_m + [\boldsymbol{K}_{mb} + \boldsymbol{K}1_{mb}]\boldsymbol{W}_b + \boldsymbol{K}_m\boldsymbol{W}_m = \boldsymbol{P}_{m\Delta T} - \boldsymbol{H}_{mq}Q \tag{39}$$

$$L\ddot{Q} + R\dot{Q} + \left(1/C_p^S\right)Q = -\left[\boldsymbol{H}_{bq}^T - \boldsymbol{H}1_{bq}^T(\boldsymbol{W}_b)\right]\boldsymbol{W}_b - \boldsymbol{H}_{mq}^T\boldsymbol{W}_m \tag{40}$$

Equations (38) and (39) describe the equilibrium equations of motion for the integrated system with a piezoelectric material whose forces are $\boldsymbol{H}_{bq}$ and $\boldsymbol{H}_{mq}$. The mechanical vibration of the piezoelectric material produces the electrical charges of the piezoelectric material, and these charges induce the piezoelectric force that suppresses the vibration of structure. Equation (40) represents the electric circuit, which consists of inductor–resistor–capacitor (L–R–C) elements in series and clearly shows that mechanical deformation generates the induced voltage $\boldsymbol{H}^T\boldsymbol{W}$ across the electrodes of piezoelectric material.

The system equations of motion in form of block matrices can be expressed as follows.

Active control:

$$\begin{bmatrix}\boldsymbol{M}_b & \boldsymbol{0}\\ \boldsymbol{0} & \boldsymbol{M}_m\end{bmatrix}\begin{Bmatrix}\ddot{\boldsymbol{W}}_b\\ \ddot{\boldsymbol{W}}_m\end{Bmatrix} + \begin{bmatrix}\boldsymbol{G} & \boldsymbol{0}\\ \boldsymbol{0} & \boldsymbol{0}\end{bmatrix}\begin{Bmatrix}\dot{\boldsymbol{W}}_b\\ \dot{\boldsymbol{W}}_m\end{Bmatrix} + \left(\begin{bmatrix}\lambda\boldsymbol{A} & \boldsymbol{0}\\ \boldsymbol{0} & \boldsymbol{0}\end{bmatrix} + \begin{bmatrix}\boldsymbol{K}_b & \boldsymbol{K}_{bm}\\ \boldsymbol{K}_{mb} & \boldsymbol{K}_m\end{bmatrix} + \begin{bmatrix}\boldsymbol{K}_{Ne} & \boldsymbol{0}\\ \boldsymbol{0} & \boldsymbol{0}\end{bmatrix} + \begin{bmatrix}\boldsymbol{K}_{N\Delta T} & \boldsymbol{0}\\ \boldsymbol{0} & \boldsymbol{0}\end{bmatrix} + \begin{bmatrix}\boldsymbol{K}1_{bbb}(\boldsymbol{W}_b) + \boldsymbol{K}1_{bbm}(\boldsymbol{W}_m) & \boldsymbol{K}1_{bm}(\boldsymbol{W}_b)\\ \boldsymbol{K}1_{mb}(\boldsymbol{W}_b) & \boldsymbol{0}\end{bmatrix} + \begin{bmatrix}\boldsymbol{K}2_b\left(\boldsymbol{W}_b^2\right) & \boldsymbol{0}\\ \boldsymbol{0} & \boldsymbol{0}\end{bmatrix}\right)\begin{Bmatrix}\boldsymbol{W}_b\\ \boldsymbol{W}_m\end{Bmatrix} = \begin{Bmatrix}\boldsymbol{P}_{b\Delta T}\\ \boldsymbol{P}_{m\Delta T}\end{Bmatrix} + \begin{Bmatrix}\boldsymbol{P}_{be}\\ \boldsymbol{P}_{me}\end{Bmatrix} \tag{41}$$

Passive damping:

$$\begin{bmatrix}\boldsymbol{M}_b & \boldsymbol{0} & \boldsymbol{0}\\ \boldsymbol{0} & \boldsymbol{M}_m & \boldsymbol{0}\\ \boldsymbol{0} & \boldsymbol{0} & L\end{bmatrix}\begin{Bmatrix}\ddot{\boldsymbol{W}}_b\\ \ddot{\boldsymbol{W}}_m\\ \ddot{Q}\end{Bmatrix} + \begin{bmatrix}\boldsymbol{G} & \boldsymbol{0} & \boldsymbol{0}\\ \boldsymbol{0} & \boldsymbol{0} & \boldsymbol{0}\\ \boldsymbol{0} & \boldsymbol{0} & R\end{bmatrix}\begin{Bmatrix}\dot{\boldsymbol{W}}_b\\ \dot{\boldsymbol{W}}_m\\ \dot{Q}\end{Bmatrix} + \left(\begin{bmatrix}\lambda\boldsymbol{A} & \boldsymbol{0} & \boldsymbol{0}\\ \boldsymbol{0} & \boldsymbol{0} & \boldsymbol{0}\\ \boldsymbol{0} & \boldsymbol{0} & \boldsymbol{0}\end{bmatrix} + \begin{bmatrix}\boldsymbol{K}_b & \boldsymbol{K}_{bm} & \boldsymbol{H}_{bq}\\ \boldsymbol{K}_{mb} & \boldsymbol{K}_m & \boldsymbol{H}_{mq}\\ \boldsymbol{H}_{bq}^T & \boldsymbol{H}_{mq}^T & 1/C_p^S\end{bmatrix} + \begin{bmatrix}\boldsymbol{K}_{N\Delta T} & \boldsymbol{0} & \boldsymbol{0}\\ \boldsymbol{0} & \boldsymbol{0} & \boldsymbol{0}\\ \boldsymbol{0} & \boldsymbol{0} & 0\end{bmatrix} + \begin{bmatrix}\boldsymbol{K}1_{bbq}(\boldsymbol{Q}) & \boldsymbol{0} & \boldsymbol{0}\\ \boldsymbol{0} & \boldsymbol{0} & \boldsymbol{0}\\ \boldsymbol{0} & \boldsymbol{0} & 0\end{bmatrix} + \begin{bmatrix}\boldsymbol{K}1_{bbb}(\boldsymbol{W}_b) + \boldsymbol{K}1_{bbm}(\boldsymbol{W}_m) & \boldsymbol{K}1_{bm}(\boldsymbol{W}_b) & \boldsymbol{H}1_{bq}(\boldsymbol{W}_b)\\ \boldsymbol{K}1_{mb}(\boldsymbol{W}_b) & \boldsymbol{0} & \boldsymbol{0}\\ \boldsymbol{H}1_{bq}^T(\boldsymbol{W}_b) & \boldsymbol{0} & 0\end{bmatrix} + \begin{bmatrix}\boldsymbol{K}2_b\left(\boldsymbol{W}_b^2\right) & \boldsymbol{0} & \boldsymbol{0}\\ \boldsymbol{0} & \boldsymbol{0} & \boldsymbol{0}\\ \boldsymbol{0} & \boldsymbol{0} & 0\end{bmatrix}\right)\begin{Bmatrix}\boldsymbol{W}_b\\ \boldsymbol{W}_m\\ Q\end{Bmatrix} = \begin{Bmatrix}\boldsymbol{P}_{b\Delta T}\\ \boldsymbol{P}_{m\Delta T}\\ 0\end{Bmatrix} \tag{42}$$

or

$$\boldsymbol{M}\ddot{\boldsymbol{U}} + \boldsymbol{C}\dot{\boldsymbol{U}} + (\lambda\boldsymbol{A} + \boldsymbol{K} + \boldsymbol{K}_{N\Delta T} + \boldsymbol{K}_{Ne} + \boldsymbol{K}1 + \boldsymbol{K}2)\boldsymbol{U} = \boldsymbol{P}_{\Delta T} + \boldsymbol{P}_e \tag{43}$$

where $\boldsymbol{M}$, $\boldsymbol{G}$, and $\boldsymbol{K}$ are the system mass, aerodynamic damping, and linear stiffness matrices, respectively. $\boldsymbol{K}_{N\Delta T}$ and $\boldsymbol{K}_{Ne}$ are the induced geometric stiffnesses by the temperature and piezoelectric material, respectively. $\boldsymbol{K}1$ and $\boldsymbol{K}2$ are the first- and second-order nonlinear stiffness matrices, which depend linearly and quadratically on the element displacements, respectively. $\boldsymbol{P}_{\Delta T}$ is the temperature-induced load vector, and $\boldsymbol{P}_e$ is the piezoelectric load vector. $\boldsymbol{A}$ is the skew-symmetrical aerodynamic influence matrix. All element matrices are symmetric except $\boldsymbol{A}$. C_p^S is the inherent capacitance of piezoelectric materiel.

Equation (42) is derived for one piezoelectric patch, and it can be easily extended to multipiezoelectric patches. For example, in the

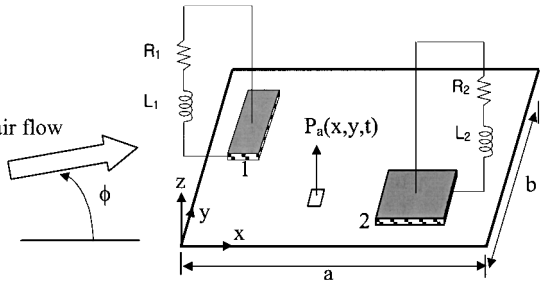

Fig. 1 Schematic diagram of a panel with two piezoelectric patches.

case of two independent piezoelectric patches of Fig. 1, Eq. (42) can be rewritten as

$$\begin{bmatrix} \boldsymbol{M}_b & \boldsymbol{0} & \boldsymbol{0} & \boldsymbol{0} \\ \boldsymbol{0} & \boldsymbol{M}_m & \boldsymbol{0} & \boldsymbol{0} \\ \boldsymbol{0} & \boldsymbol{0} & L_1 & 0 \\ \boldsymbol{0} & \boldsymbol{0} & 0 & L_2 \end{bmatrix} \begin{Bmatrix} \ddot{\boldsymbol{W}}_b \\ \ddot{\boldsymbol{W}}_m \\ \ddot{Q}_1 \\ \ddot{Q}_2 \end{Bmatrix} + \begin{bmatrix} \boldsymbol{G} & \boldsymbol{0} & \boldsymbol{0} & \boldsymbol{0} \\ \boldsymbol{0} & \boldsymbol{0} & \boldsymbol{0} & \boldsymbol{0} \\ \boldsymbol{0} & \boldsymbol{0} & R_1 & 0 \\ \boldsymbol{0} & \boldsymbol{0} & 0 & R_2 \end{bmatrix} \begin{Bmatrix} \dot{\boldsymbol{W}}_b \\ \dot{\boldsymbol{W}}_m \\ \dot{Q}_1 \\ \dot{Q}_2 \end{Bmatrix}$$

$$+ \left(\begin{bmatrix} \lambda \boldsymbol{A} & \boldsymbol{0} & \boldsymbol{0} & \boldsymbol{0} \\ \boldsymbol{0} & \boldsymbol{0} & \boldsymbol{0} & \boldsymbol{0} \\ \boldsymbol{0} & \boldsymbol{0} & 0 & 0 \\ \boldsymbol{0} & \boldsymbol{0} & 0 & 0 \end{bmatrix} + \begin{bmatrix} \boldsymbol{K}_b & \boldsymbol{K}_{bm} & \boldsymbol{H}^1_{bq} & \boldsymbol{H}^2_{bq} \\ \boldsymbol{K}_{mb} & \boldsymbol{K}_m & \boldsymbol{H}^1_{mq} & \boldsymbol{H}^2_{mq} \\ \boldsymbol{H}^1_{qb} & \boldsymbol{H}^1_{qm} & 1/C^S_{p,1} & 0 \\ \boldsymbol{H}^2_{bq} & \boldsymbol{H}^2_{qm} & 0 & 1/C^S_{p,2} \end{bmatrix} \right.$$

$$+ \begin{bmatrix} \boldsymbol{K}_{N\Delta T} & \boldsymbol{0} & \boldsymbol{0} & \boldsymbol{0} \\ \boldsymbol{0} & \boldsymbol{0} & \boldsymbol{0} & \boldsymbol{0} \\ \boldsymbol{0} & \boldsymbol{0} & 0 & 0 \\ \boldsymbol{0} & \boldsymbol{0} & 0 & 0 \end{bmatrix} + \begin{bmatrix} \boldsymbol{K}1_{bbq}(\boldsymbol{Q}) & \boldsymbol{0} & \boldsymbol{0} & \boldsymbol{0} \\ \boldsymbol{0} & \boldsymbol{0} & \boldsymbol{0} & \boldsymbol{0} \\ \boldsymbol{0} & \boldsymbol{0} & 0 & 0 \\ \boldsymbol{0} & \boldsymbol{0} & 0 & 0 \end{bmatrix}$$

$$+ \begin{bmatrix} \boldsymbol{K}1_{bbb}(\boldsymbol{W}_b) + \boldsymbol{K}1_{bbm}(\boldsymbol{W}_m) & \boldsymbol{K}1_{bm}(\boldsymbol{W}_b) & \boldsymbol{H}1^1_{bq}(\boldsymbol{W}_b) & \boldsymbol{H}1^2_{bq}(\boldsymbol{W}_b) \\ \boldsymbol{K}1_{mb}(\boldsymbol{W}_b) & \boldsymbol{0} & \boldsymbol{0} & \boldsymbol{0} \\ \boldsymbol{H}1^1_{qm}(\boldsymbol{W}_b) & \boldsymbol{0} & 0 & 0 \\ \boldsymbol{H}1^2_{qm}(\boldsymbol{W}_b) & \boldsymbol{0} & 0 & 0 \end{bmatrix}$$

$$\left. + \begin{bmatrix} \boldsymbol{K}2_b(\boldsymbol{W}_b^2) & \boldsymbol{0} & \boldsymbol{0} & \boldsymbol{0} \\ \boldsymbol{0} & \boldsymbol{0} & \boldsymbol{0} & \boldsymbol{0} \\ \boldsymbol{0} & \boldsymbol{0} & 0 & 0 \\ \boldsymbol{0} & \boldsymbol{0} & 0 & 0 \end{bmatrix} \right) \begin{Bmatrix} \boldsymbol{W}_b \\ \boldsymbol{W}_m \\ Q_1 \\ Q_2 \end{Bmatrix} = \begin{Bmatrix} \boldsymbol{P}_{b\Delta T} \\ \boldsymbol{P}_{m\Delta T} \\ 0 \\ 0 \end{Bmatrix} \tag{44}$$

V. Solution Procedure

In the development of the flutter suppression strategy, it is generally impractical to consider all modeled modes because of large degrees of freedom of the system equations of motion. This section describes the methods of modal transformation. A powerful piezoelectric force is necessary to suppress flutter effectively, and piezoceramic material (PZT) satisfies this requirement. In the design of PZT, the optimal placement of PZT is calculated to maximize the piezoelectric force, and the genetic algorithm is used in the optimization process.

Modal Equations

Equation (43) can be changed to the properly chosen modal coordinates by the following modal transformation:

$$\boldsymbol{U} = \sum_{r=1}^{m} \sum_{s=1}^{n} \boldsymbol{\eta}_{rs}(t)\{\phi_{rs}\} \tag{45}$$

where $\boldsymbol{\eta}_{rs}$ is modal displacement vector and $\{\phi_{rs}\}$ is normal mode vector, which is obtained from linear vibration analysis of the system:

$$\boldsymbol{K}\{\phi_{rs}\} = \mu \boldsymbol{M}\{\phi_{rs}\} \tag{46}$$

For a rectangular panel with zero airflow angle, it is well known that the response of panel flutter produces good results even though one consider the first few modes in the airflow direction (for example, $m = 6$) and the first mode in the spanwise direction ($n = 1$) (Ref. 10). Then, Eq. (45) becomes

$$\boldsymbol{U} = \sum_{r=1}^{m} \boldsymbol{\eta}_r(t)\{\phi_r\} = \boldsymbol{\Phi}\boldsymbol{\eta} \tag{47}$$

A normalization of the orthogonality condition for the eigenvectors ($\boldsymbol{\Phi}^T \boldsymbol{M} \boldsymbol{\Phi} = \boldsymbol{I}$) is adopted, and the substitution of Eq. (47) into Eq. (43) gives the nonlinear modal equations

$$\boldsymbol{\eta}_{,\tau\tau} + \tilde{\boldsymbol{C}}\boldsymbol{\eta}_{,\tau} + (\tilde{\boldsymbol{K}} + \tilde{\boldsymbol{K}}_{Ne} + \tilde{\boldsymbol{K}}_{\eta} + \tilde{\boldsymbol{K}}_{\eta\eta})\boldsymbol{\eta} = \tilde{\boldsymbol{P}}_{\Delta T} + \tilde{\boldsymbol{P}}_e \tag{48}$$

where $\tau = \omega_0 t$ is the nondimensional time variable and modal stiffness matrices and modal thermal force vector are expressed as follows:

$$\tilde{\boldsymbol{K}} = \boldsymbol{\Phi}^T(\lambda \boldsymbol{A} + \boldsymbol{K} + \boldsymbol{K}_{N\Delta T})\boldsymbol{\Phi}, \qquad \tilde{\boldsymbol{K}}_{Ne} = \boldsymbol{\Phi}^T \boldsymbol{K}_{Ne} \boldsymbol{\Phi}$$

$$\tilde{\boldsymbol{K}}_{\eta} = \boldsymbol{\Phi}^T \boldsymbol{K}1 \boldsymbol{\Phi}, \qquad \tilde{\boldsymbol{K}}_{\eta\eta} = \boldsymbol{\Phi}^T \boldsymbol{K}2 \boldsymbol{\Phi}$$

$$\tilde{\boldsymbol{P}}_{\Delta T} = \boldsymbol{\Phi}^T \boldsymbol{P}_{\Delta T}, \qquad \tilde{\boldsymbol{P}}_e = \boldsymbol{\Phi}^T \boldsymbol{P}_e = \boldsymbol{\Phi}^T \boldsymbol{F}_{\mathrm{PZT}} \boldsymbol{V}_a \tag{49}$$

The reduced nonlinear modal equation of motion, Eq. (48), is solved using a time numerical integration method such as the Newmark-β method.

Optimal Shape and Location of PZT

In the design of PZT patches, the optimal shape and the location of PZT is calculated to maximize the actuating force, when the number and the size of PZT are given. When an element is covered with PZT, that element turns on. When an element is not covered with PZT, that element turns off. That on and off of each element is determined by using the genetic algorithm.[7]

For the active control method, the performance index to be maximized is

$$\text{maximize: } \min\left(\left| \boldsymbol{\Phi}_c^T \boldsymbol{F}_{\mathrm{PZT}} \right| \right) \tag{50}$$

where $\boldsymbol{\Phi}_c^T \boldsymbol{F}_{\mathrm{PZT}}$ is the modal actuating forces for the controlled modes.

For the passive suppression scheme, the damping performance induced by the piezoelectric patch is enhanced as the piezoelectric force $\boldsymbol{HQ}$ is increased. Additionally, larger induced voltage $\boldsymbol{H}^T\boldsymbol{W}$ increases the dissipation of electric energy through the resistor in the electric circuit. Moreover, the damping performance can be effectively enhanced if the electromechanical coupling matrix $\boldsymbol{H}$ is designed to increase the piezoelectric force corresponding to the modes that are to be suppressed. Note that the electromechanical coupling matrix $\boldsymbol{H}$ depends on the location of piezoelectric patch, as well as the piezoelectric material property h_{31}. Therefore, it is desirable to place the piezoelectric patch at the location to maximize the modal piezoelectric force. The performance index used in the optimized process is defined by

$$\text{maximize: } \left| \boldsymbol{\Phi}_c^T \boldsymbol{H} \right| \tag{51}$$

where $\boldsymbol{\Phi}_c^T \boldsymbol{H}$ is associated with the modal piezoelectric force per unit charge.

After the optimal shape and the location of piezoelectric patch are determined, the optimum magnitudes of resistance and inductance must be determined, and those values can be obtained by a pole placement method.[3]

Controller Design: Active Control

The linearized model is obtained by ignoring the nonlinear terms and thermal load from Eq. (48) (Ref. 2):

$$\boldsymbol{\eta}_{,\tau\tau} + \tilde{\boldsymbol{C}}\boldsymbol{\eta}_{,\tau} + (\tilde{\boldsymbol{K}} + \tilde{\boldsymbol{K}}_{Ne})\boldsymbol{\eta} = \boldsymbol{\Phi}^T \boldsymbol{F}_{\mathrm{PZT}} \boldsymbol{V}_a \tag{52}$$

A linear optimal control theory is designed for the active control method. The structural model is transformed into a state-space model such as

$$\dot{\boldsymbol{X}} = \boldsymbol{A}\boldsymbol{X} + \boldsymbol{B}\boldsymbol{V}_a \tag{53}$$

where state vector $X = [\eta, \dot{\eta}]$ and system matrix

$$A = \begin{bmatrix} 0 & I \\ -(\tilde{K} + \tilde{K}_{Ne}) & -\tilde{C} \end{bmatrix}$$

control influence coefficient matrix $B = [0 \;\; \Phi^T \;\; F_{PZT}]^T$, and control input $V_a = V_3 / V_{3\max}$.

The linear quadratic performance index applied for finding the optimal control can be expressed as

$$J = \frac{1}{2} \int_0^\infty \left(X^T Q X + V_a^T R V_a \right) d\tau \tag{54}$$

where Q and R are state penalty matrix and control penalty matrix, respectively.

The optimal controller is $V_a = -R^{-1} B^T P X$, based on the optimal control theory, where the P matrix is obtained from the Riccati equation

$$A^T P + PA - PBR^{-1} B^T P = -Q \tag{55}$$

VI. Numerical Results

As the verification example, a simply supported square graphite/epoxy panel of eight layers $[0/45/-45/90]_s$ is investigated.[11] At critical buckling temperature $\Delta T / \Delta T_{cr} = 1.0$ and $\lambda = 450$, the panel motion is a limit cycle as shown in Fig. 2.

The active and the passive suppressions of nonlinear panel flutter are experimented numerically. The six-coupled nonlinear modal equations are integrated by using the Newmark-β method, and responses of panel motion are presented at location $x = 0.75a$ and $y = 0.5b$. For the analyses, a simply supported $[45/-45/90/0]_s$ square graphite/epoxy composite plate is modeled, and the critical dynamic pressure λ_{cr} and critical buckling temperature ΔT_{cr} of the composite plate are found to be 205 and 19.07°C, respectively.

The material properties of graphite/epoxy composite and piezoelectric materials are summarized in Table 1. The dimensions of the composite plate are 0.3 m × 0.3 m × 0.001 m. The nonuniform temperature distribution in the examples is assumed as $\Delta T = T_0 \sin(\pi x/a) \sin(\pi y/b)$, and the aerodynamic damping coefficient is assumed to be $\mu / M_\infty = 0.01$.

Table 1 Material properties

Property	Graphite/epoxy	PZT (PSI-5A4E)
Elastic property	——	——
E_1, GPa	155	66
E_2, GPa	8.07	66
G_{12}, GPa	4.55	25.38
v_{12}	0.22	0.31
Coupling coefficient (k_{31})	0	0.32
Thermal expansion, 10^{-6}/°C	——	——
α_1	−0.07	4
α_2	30.1	4
Piezoelectric coefficient	——	——
d_{31}	0	-190×10^{-12} m/V
h_{31}	0	-1.622×10^9 N/C
Electric permittivity	——	——
$\in_{33}^T / \in_0$	0	1800
($\in_0 = 8.85 \times 10^{-12}$ F/m)	——	——
Maximum electric field, 10^5 V/m	0	5.0
Mass density, kg/m^3	1550	7800

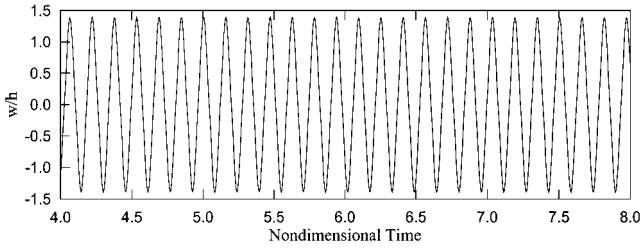

Fig. 2 Limit-cycle motions of a simply supported square $[0/45/-45/90]_s$ panel ($\mu/M_\infty = 0.01$) at $\lambda = 450$ and $\Delta T/\Delta T_{cr} = 1.0$.

Figure 3 shows the piezoelectric patch configuration used to suppress the first flutter mode, and the frequency of the first mode (1, 1) is 64.07 Hz. The (1, 1) mode shape is shown in Fig. 4.

The piezoelectric patch is bonded at the bottom side of the panel to avoid the extrusion on the airflow side, and the piezoelectric layer thickness is assumed as 0.0005 m.

In Fig. 5, the modal frequency and the damping of the panel are calculated as a function of inductance L at a fixed resistance ($R = 3899\ \Omega$). It is found that maximum shifts of the modal frequencies occur near the point of optimal inductance that produces the maximum damping.

In Fig. 6, the modal frequency and the damping of the flutter mode (1, 1) are calculated as a function of resistance at fixed optimal inductance value (25 H) obtained from Fig. 5. It is observed that the frequency at low resistance is gradually reduced to the short-circuit condition and the frequency converges to open-circuit condition as the resistance is increased. It is also observed that maximum shift of modal frequency occurs near the point of maximum damping as in the earlier case.

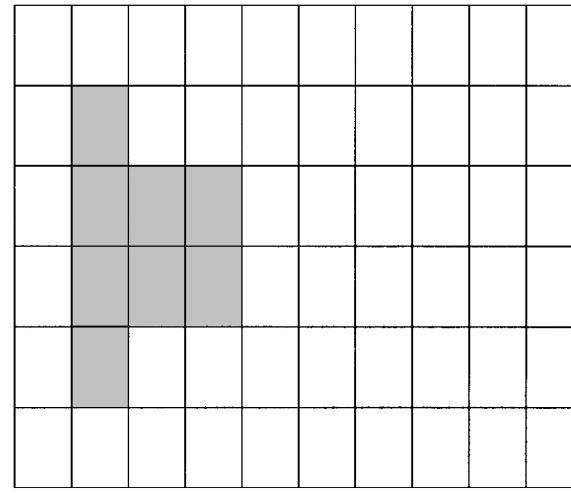

Fig. 3 Shape and the location of piezoceramic patch.

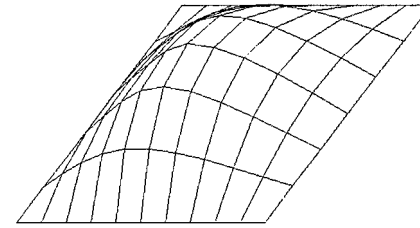

Fig. 4 First mode (1, 1) shape.

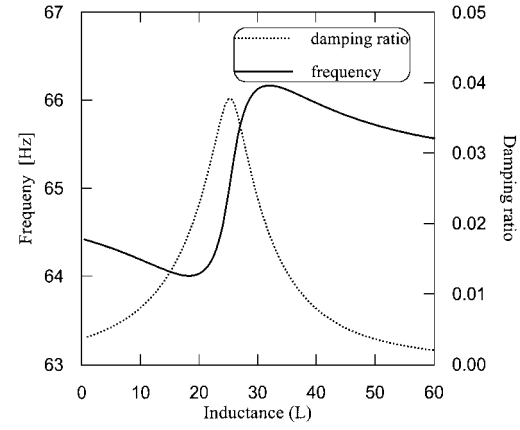

Fig. 5 Effects of inductance on the modal frequency and damping for first flutter mode (1, 1); $R = 3899\ \Omega$.

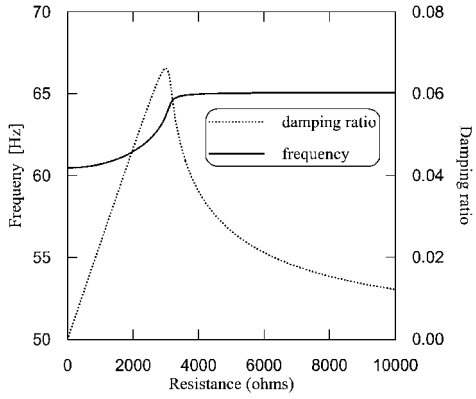

Fig. 6 Effects of resistance on the modal frequency and damping for first flutter mode (1, 1); $L = 25$ H.

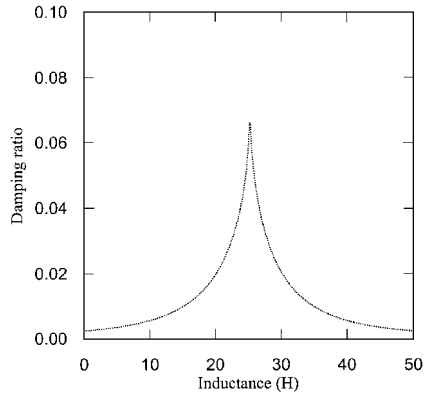

Fig. 7 Effects of inductance on the modal frequency and damping for first flutter mode (1, 1); $R = 2800\ \Omega$.

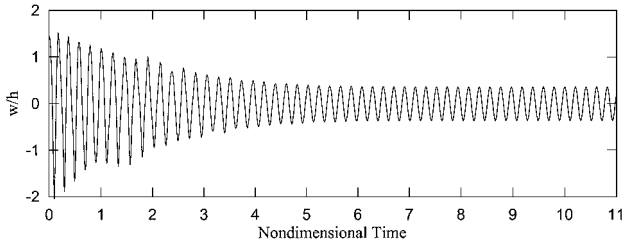

Fig. 8 Time history of panel motion at short circuit condition; $\Delta T = 0$ and $\lambda = 290$.

In Fig. 7, the modal frequency and the damping of the flutter mode (1, 1) are calculated as a function of inductance at fixed optimal resistance value (2800 Ω) obtained from Fig. 6. Larger portions of electrical energy are dissipated in the resistor during a vibration cycle when the optimal inductance and resistance are realized.

The panel motions at short condition, active control, and passive suppression are studied based on the PZT patch shown in Fig. 3. Figure 8 shows that the panel motion at short-circuit condition becomes a limit-cycle vibration under the dynamic pressure $\lambda = 290$ without thermal load. Time history and control voltage for active control are shown in Fig. 9. The flutter motion is shown to be suppressed by the piezoelectric actuation within several cycles after the controller is activated. With optimal resistance (2.8 kΩ) and inductance (25 H), the limit cycle can be suppressed completely, as shown in Fig. 10.

Next, we design the suppression system with two independent sets of piezoceramic patches for multimodal suppression. To obtain the optimal shape and location of the piezoceramic patch, the genetic algorithm is implemented in the developed computer program. During the design of the piezoceramic patches, it is assumed that the size and the number of piezoceramic patches are constant, and the number of piezoceramic patch is six for each mode in the Fig. 11.

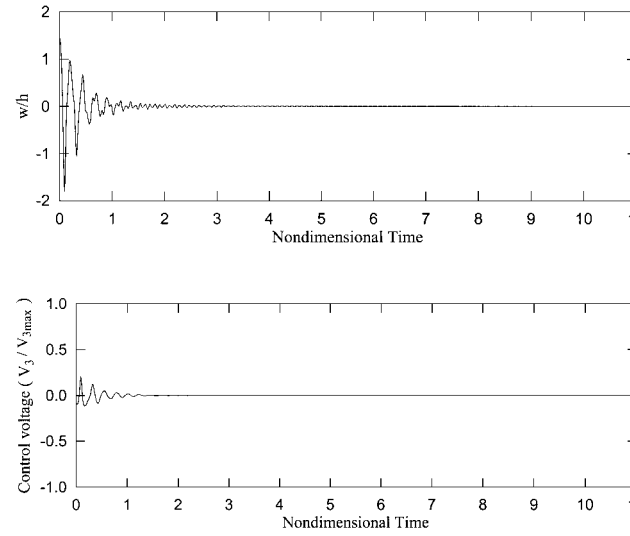

Fig. 9 Time history of panel motion and control input at active control; $\Delta T = 0$ and $\lambda = 290$.

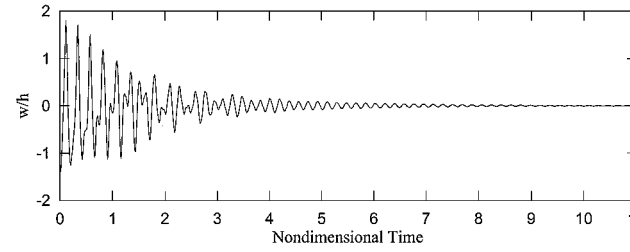

Fig. 10 Time history of panel motion with shunted circuit of $L = 25$ H and $R = 2.8$ kΩ at passive suppression; $\Delta T = 0$ and $\lambda = 290$.

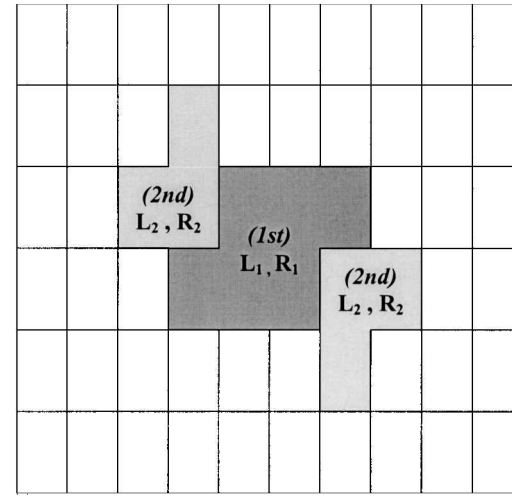

Fig. 11 Optimal shape and location of piezoceramic patches.

The darker area is the optimal patch shape for the first flutter mode (1, 1), and the lighter area is the optimal patch shape for the second flutter mode (2, 1). Population in one generation is set to 600, and 0.6 of crossover probability and 0.03 of mutation probability are used in the genetic algorithm. Each independent piezoelectric element is connected with an L–R series circuit.

Time histories and control input in the case of $\lambda = 400$ and no thermal load are shown in Figs. 12 and 13. The panel motion becomes a limit cycle at the short-circuit condition, and the limit-cycle motion is shown to be completely suppressed within several cycles after the controller is activated, as shown in Figs. 12. Figure 13 shows that the limit-cycle oscillation can be suppressed completely by two-resonant shunt circuits with $L_1 = 27.49$ and $L_2 = 4.93$ H and $R_1 = 1653$ and $R_2 = 787$ kΩ.

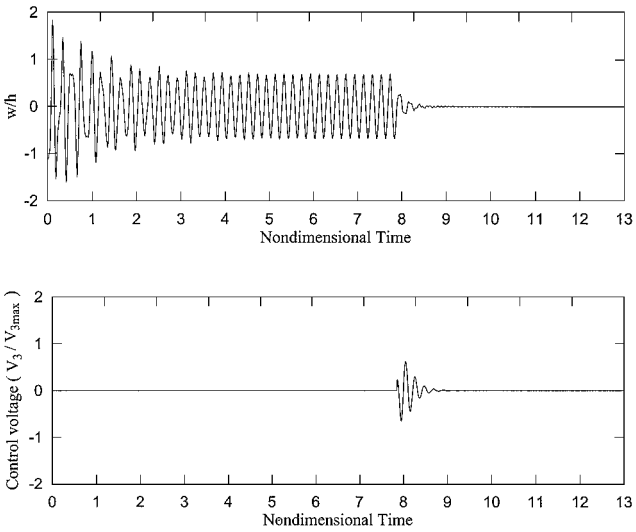

Fig. 12 Time history of panel motion and control input at active control; $\Delta T = 0$ and $\lambda = 400$.

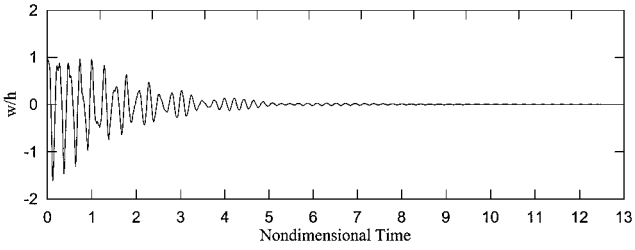

Fig. 13 Time history of panel motion with shunted circuits of $L_1 = 27.49$ H, $L_2 = 4.93$ H, $R_1 = 1653$ kΩ, and $R_2 = 787$ kΩ at passive suppression; $\Delta T = 0$ and $\lambda = 400$.

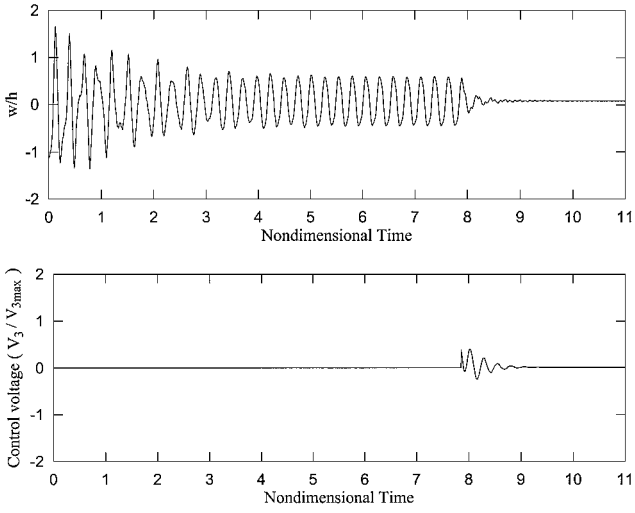

Fig. 14 Time history of panel motion and control input at active control; $T_0 = 20°$ C and $\lambda = 250$.

Flutter suppression is also investigated as the thermal load increased. The time histories and control effort at $T_0 = 20°$C are shown in Figs. 14 and 15. The panel motion becomes a limit cycle at the short-circuit condition, and the limit-cycle motion is shown to be completely suppressed by active control. With shunt circuits, the peak amplitude of the limit cycle reduces by about 60%.

The time histories and control effort at $T_0 = 30°$C are shown in Figs. 16 and 17. The limit-cycle motion at the short circuit is shown to be completely suppressed by active control, and the peak amplitude of the limit cycle reduces by about 30% with shunt circuits. The limit-cycle motion at low temperature and certain dynamic pressure can be completely suppressed. However, as the temperature increased, limit-cycle motion cannot be completely suppressed with the limited piezoelectric force.

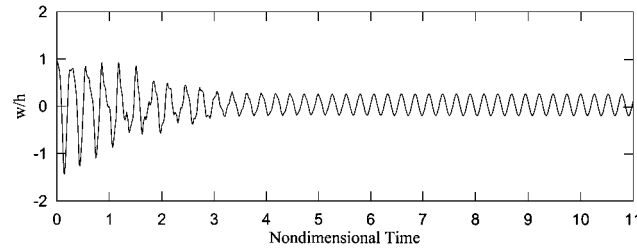

Fig. 15 Time history of panel motion with shunted circuits of $L_1 = 27.49$ H, $L_2 = 4.93$ H, $R_1 = 1653$ kΩ, and $R_2 = 787$ kΩ, $T_0 = 20°$C and $\lambda = 250$, at passive suppression.

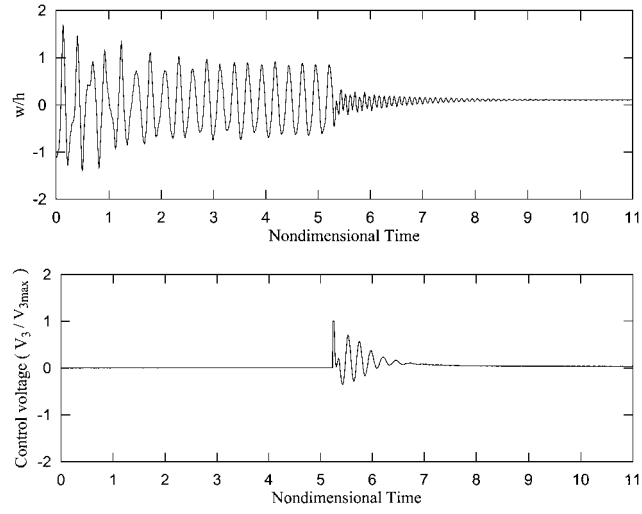

Fig. 16 Time history of panel motion and control input at active control; $T_0 = 30°$ C and $\lambda = 250$.

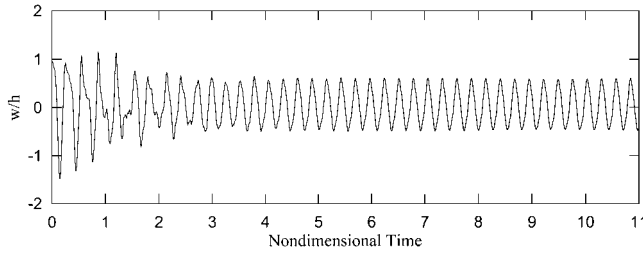

Fig. 17 Time history of panel motion with shunted circuits of $L_1 = 27.49$ H, $L_2 = 4.93$ H, $R_1 = 1653$ kΩ, and $R_2 = 787$ kΩ, $T_0 = 20°$C and $\lambda = 250$, at passive suppression.

VII. Conclusions

An active control method based on the linear optimal control theory and passive suppression schemes using multi L–R series shunt circuits for nonlinear panel flutter is investigated. The governing equation of a piezoelectric passive damper and finite element formulation are newly derived. The optimal shape and location that maximizes piezoelectric force is determined by using genetic algorithms. With the use of the Newmark-β method, the effects of active and passive suppression for composite panel flutter are investigated at various temperature and dynamic pressure conditions in the time domain. The limit-cycle motion at low temperature and certain dynamic pressure can be completely suppressed. However, as the temperature increased, limit-cycle motion cannot be completely suppressed with the limited piezoelectric force. The performance of passive damping is decreased at a higher temperature than that of active control. Further studies at a higher temperature condition are needed. However, note that there is no need for additional apparatuses such as sensor and power equipment in the passive damping scheme, and there is also no need for a control instruments.

Therefore, practically speaking, the passive damping suppression scheme can be preferable for the panel flutter.

Acknowledgment

This study has been supported by the Ministry of Science and Technology through the National Research Laboratory Program (Contract 2000-N-NL-01-C-026).

References

[1]Scott, R. C., and Weisshaar, T. A., "Controlling Panel Flutter Using Adaptive Materials," *Journal of Aircraft*, Vol. 31, No. 1, 1994, pp. 213–222.

[2]Zhou , R. C., Lai, Z., Xue, D. Y., Hauang, J.-K., and Mei, C., "Suppression of Nonlinear Panel Flutter with Piezoelectric Actuators Using Finite Element," *AIAA Journal*, Vol. 33, No. 6, 1995, pp. 1098–1105.

[3]Hagood, N. W., and Von Flotow, A. V., "Damping of Structural Vibrations with Piezoelectric Materials and Passive Electrical Networks," *Journal of Sound and Vibration*, Vol. 146, No. 2, 1991, pp. 243–268.

[4]Hollkamp, J. J., "Multimodal Passive Vibration Suppression with Piezoelectric Materials and Resonant Shunts," *Journal of Intelligent Material Systems and Structures*, Vol. 5, No. 1, 1994, pp. 49–57.

[5]Tang, J., Wang, K. W., and Philen, M., "Sliding Mode Control of Structural Vibrations via Active–Passive Hybrid Piezoelectric Network," *Smart Structures and Integrated Systems*, *Proceedings of SPIE Smart Structures and Materials*, Vol. 3668, Society of Photo-Optical Instrumentation Engineers, Bellingham, WA, 1999, pp. 543–553.

[6]Hollkamp, J. J., and Gorden, R. W., "An Experimental Comparison of Piezoelectric and Constrained Layer Damping," *Smart Structures and Integrated Systems*, *Proceedings of SPIE Smart Structures and Materials*, Vol. 2445, Society of Photo-Optical Instrumentation Engineers, Bellingham, WA, 1995, pp. 123–133.

[7]Kim, S. J., Han, C. H., and Yun, C. Y., "Improvement of Aeroelastic Stability of Hingeless Helicopter Rotor Blade by Passive Piezoelectric Damping," *Smart Structures and Integrated Systems*, *Proceedings of SPIE Smart Structures and Materials*, Vol. 3672, Society of Photo-Optical Instrumentation Engineers, Bellingham, WA, 1999, pp. 131–141.

[8]Bathe, K. J., *Finite Element Procedures*, Prentice–Hall International, Upper Saddle River, NJ, 1996, pp. 768–837.

[9]Goldberg, D. E., *Genetic Algorithms in Search, Optimization and Machine Learning*, Addison Wesley Longman, Reading, MA, 1989.

[10]Dowell, E. H., "Nonlinear Oscillations of a Fluttering Plate," *AIAA Journal*, Vol. 4, No. 7, 1966, pp. 1267–1275.

[11]Zhou, R. C., Lai, Z., Xue, D. Y., and Mei, C., "Finite Time Domain-Modal Formulation for Nonlinear Flutter of Composite Panels," *AIAA Journal*, Vol. 32, No. 10, 1994, pp. 2044–2052.

A. M. Baz
Associate Editor